ISSN 1054-660X, Laser Physics, 2009, Vol. 19, No. 4, pp. 647–654.

Vortex Lattice of a Bose–Einstein Condensate as a Photonic Band Gap Material[1]

M. E. Taşgın[a], Ö. E. Müstecaplıoğlu[b], and M. Ö. Oktel[a]

[a] *Department of Physics, Bilkent University, Bilkent, Ankara, 06800 Turkey*
[b] *Department of Physics, Koç University, Sartyer, Istanbul, 34450 Turkey*
e-mail: omustecap@ku.edu.tr
Received November 21, 2008

Abstract—Photonic crystal behavior of a rotating Bose–Einstein condensate with a triangular vortex lattice is reviewed and a scheme for getting much wider band gaps is proposed. It is shown that photonic band gaps can be widened an order of magnitude more by using a Raman scheme of index enhancement, in comparison to previously considered upper level microwave scheme.

PACS numbers: 03.75.Lm, 42.50.Gy, 42.70.Qs, 74.25.Qt

DOI: 10.1134/S1054660X09040197

1. INTRODUCTION

When a Bose–Einstein condensate (BEC) is rotated, after a certain critical frequency, vortices start to form. For high enough rotation frequency, these vortices become large in number and distribute in a periodical structure [1–4]. The usual structure is a triangular lattice, but other lattice types may as well occur, depending on the strength of the inter-particle interactions [5]. The density profile is periodically distributed vortices on an envelope function, which decreases toward the edge of the condensate [3, 4]. The envelope is a slowly varying function compared to the vortex periodicity, such that few hundred vortices are observable experimentally [6]. The imaging of the lattice was accomplished while the condensate is in the trap in [5], different from the usual ballistic expansion imaging [1, 2, 7–9].

This periodicity simulates 2D photonic band gap (PBG) materials. Despite the common PBG material [10], however, the lattice parameter of a BEC vortex lattice is continuously tunable via the rotation frequency. Moreover, lattice type can be changed, while the BEC is in the trap, by controlling the inter-particle interaction strength by Feshbach resonances [11].

We recently proposed [12, 13] to directly measure the rotation frequency of BEC using the reflection from a directional PBG pulse propagation, stopped only in certain directions and allowed in others. The chopping in the reflected pulse, propagating through BEC lattice, measures its rotation frequency.

The difficulty is, however, to establish the high enough index contrast between the vortex cores and the bulk of the BEC. BEC is dilute gaseous atomic medium, as such exhibits dispersion and polarization only in the high absorptive frequency regimes. Necessary contrast is achieved using one of the index-enhancement schemes [14, 15], which are based on the atomic quantum coherence. Coupling the excited (or ground) state to other auxiliary levels, it is possible to obtain high polarization response without absorption [15]. Quantum interference of various absorption paths allows the retain of the atoms in the excited level with cancelling absorption.

Dielectric response, obtained using index enhancement schemes, is complex in structure. Gain and absorption regimes crossover the zero absorption frequency and more over they are very strong (see Fig. 2). Dielectric function varies rapidly with the frequency and both real and imaginary parts of it changes sign. Checking the existence of the PBG at exactly on the zero-absorption frequency is straightforward. However, the determination of the frequency width of the band gap about such a point, surrounded by both gain and absorption, is sophisticated [13].

In this paper, we examine the photonic band structure of a triangular vortex lattice. We investigate the frequency width of the photonic band gap, for a complex frequency-dependent dielectric function. The unusual dielectric response is due to the index enhancement scheme [14], which is utilized for high index contrast. In order to be able to determine the band gap width, we also examine the complex Poynting vector beside the complex wave vector. We first review our previous results [12, 13] based upon upper level microwave scheme for index enhancement. After that we shall consider Raman scheme and show that it is capable to generate much wider band gaps.

Although in the literature there exists abundant of studies on photonic crystals (PC), the ones considering the complex frequency-dependent dielectric function are rare. There exist few studies, but these are focused on the examination of the effects of metallic compo-

[1] The article is published in the original.

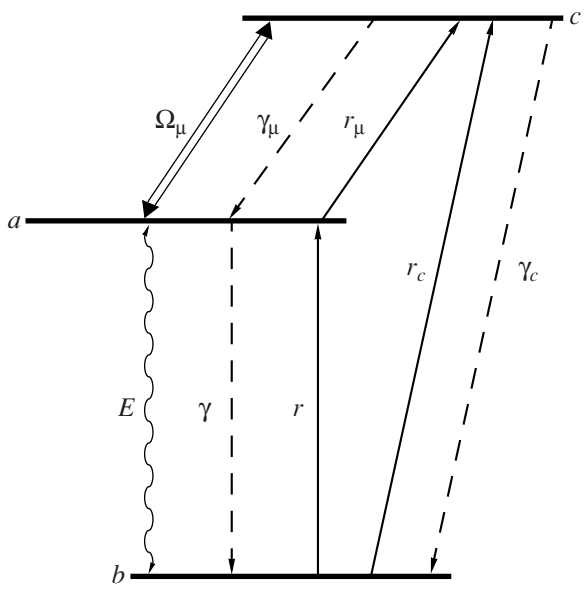

Fig. 1. Upper-level microwave scheme for index enhancement [14]. Upper two levels *a* and *c* are coupled via a strong microwave field of Rabi frequency Ω_μ. Weak probe field *E*, of optical frequency ω is coupled to levels *a* and *b*. Decay (γ) and pump (*r*) rates are indicated.

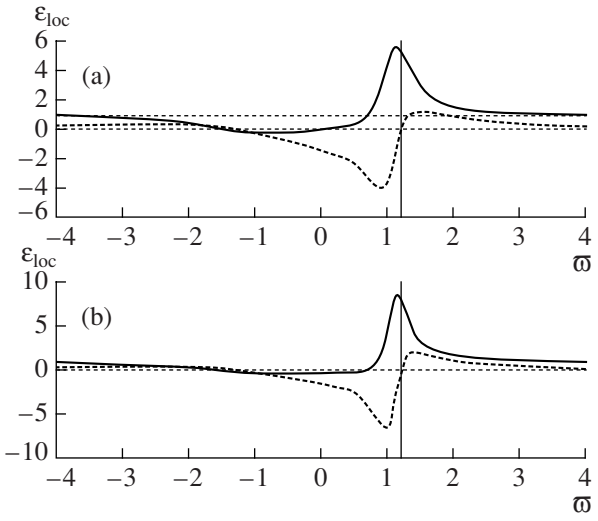

Fig. 2. Real (solid-line) and imaginary (doted-line) parts of local dielectric function $\epsilon_{loc}(\omega)$ as a function of scaled frequency $\varpi = (\omega - \omega_{ab})/\gamma$, for the particle densities (a) $N = 5.5 \times 10^{20}$ and (b) 6.6×10^{20} m^{-3}. Vertical solid line indicates the scaled enhancement frequency $\varpi_0 \simeq 1.22$, where $\epsilon''_{loc}(\varpi)$ vanishes. (a) $\epsilon = \epsilon_{loc}(\varpi_0) = 5.2$ and (b) 8.0.

nents to the bands of PC [16–22]. In the widely used Drude model, absorption is of negligible importance in the transparency window. Small, but realistic, amount of absorption does not change the band structure much [18]. On the other hand in the region of appreciable absorption there may occur no gap [21].

The dielectric function, we deal here, is completely different then the ones considered up to present. BEC offers gain regimes, as well as absorptive, beyond the enhancement window [14], which resembles the lasing without inversion [15]. To our knowledge, PBG of such a periodic structure, composed of index-enhanced media, is investigated in [13] for the first time. The gain regime is important for the understanding of the lasing properties of PC [23], as well as absorptive properties are advantageous in various applications [24].

The paper is organized as follows. In Section 2 we describe the dielectric function $\epsilon(\mathbf{r}, \omega)$ inside the vortex PC, that is enhanced with upper-level microwave scheme [14]. In Section 3, we deduce the matrix equations from the master equation of PC. We show how to obtain the band structure for a complex frequency-dependent dielectric susceptibility. In Section 4.1 we present the resulting photonic bands for two different lattice constants. In Section 4.2 we discuss the frequency width of the band gap in the presence of gain and absorption. In Section 5 we present the band results for Raman index enhancement scheme. We summarize our results in Section 6.

2. DIELECTRIC FUNCTION OF THE VORTEX LATTICE

Among the various index enhancement schemes [14], upper-level microwave scheme (see Fig. 1) leads to the strongest index contrast with vanishing absorption (Fig. 2). Another one is the Raman scheme [14], discussed in Section 5, generates weaker enhancement, but in a broader frequency window. The former one results in stronger stoppage at a single frequency, while the later operates as a weaker blocker at broader frequency range.

In the upper-level microwave scheme, the excited level *a* is coupled to an auxiliary level *c* via a strong resonant microwave field of Rabi frequency Ω_μ. The weak optical field *E*, coupling the ground state *b* to excited state *a*, is the test field. Its dielectric response is calculated. Alternative absorption path $b \longrightarrow c \longrightarrow a$ destructively interfere with the direct absorption path $b \longrightarrow a$ [15]. This quantum interference, due to the phase difference, cancel the absorption of the probe pulse *E* at a certain frequency, plotted in Fig. 2. At the same time, high polarization is obtained by keeping population at the excited level *a*.

Upper-microwave scheme, for $r_c = \Omega_\mu = \gamma$, results in the complex dielectric susceptibility $\chi(\omega) = \chi'(\omega) + i\chi''(\omega)$ of real χ' and imaginary parts χ'' are [14]

$$\chi'(\varpi) = \frac{12N\lambda^3}{13\pi^2}\frac{\varpi}{9 - 3\varpi^2 + 4\varpi^4}, \qquad (1)$$

$$\chi''(\varpi) = -\frac{3N\lambda^3}{13\pi^2}\frac{-3+2\varpi^2}{9-3\varpi^2+4\varpi^4}, \quad (2)$$

where λ is the wavelength of the $a \longrightarrow b$ transition, and N is the number density of the particles. ϖ is the negative detuning, scaled with the decay rate of decoherence γ.

Since (1) and (2) are valid for the interaction of the field single atom, we also perform the local field correction [25] as $\chi_{loc}(\varpi) = \frac{\chi(\varpi)}{1-\chi(\varpi)/3}$. The real and imaginary parts of dielectric function $\epsilon_{loc}(\varpi) = 1 + \chi_{loc}(\varpi)$ are plotted in Fig. 2, for Rubidium-87 gas. $\Omega_0 = 2.37 \times 10^{15}$ Hz is the zero absorption frequency which corresponds to $\varpi_0 = (\Omega_0 - \omega_{ab})/\gamma \simeq 1.22$ in scaled form.

The physical levels corresponding to b, a, and c are $5s_{1/2}$, $5p_{1/2}$, and $6s_{1/2}$ fine-structure levels of Rb-87. Transition wavelengths are $\lambda = 794$ nm and $\lambda_\mu = 1.32$ μm for the probe and the microwave fields, respectively. The life time of the excited level a ($5p_{1/2}$) is 27 ns, which gives a decay rate $\gamma = 2\pi \times 6$ MHz.

The spatial periodicity of the dielectric response is simulated with hexagonal Wigner–Seitz unit cells, each including a vortex at the center and evolve to bulk at the corners. We use the Padé's analytical form [26]

$$\rho(r) = \frac{r^2(0.3437 + 0.0286r^2)}{1 + 0.3333r^2 + 0.0286r^4}, \quad (3)$$

where r is scaled with the coherence length $\xi = 1/\sqrt{8\pi N a_{sc}}$. This density behavior is valid in one unit cell. $\rho(r)$ becomes zero at the center and approaches to 1 towards the edges of the hexagon. The dielectric function becomes

$$\epsilon_{loc}(\mathbf{r}, \varpi) = 1 + \rho(\mathbf{r})\chi_{loc}(\varpi) \quad (4)$$

inside one unit cell and repeats itself within the triangular lattice periodicity.

3. CALCULATION OF THE PHOTONIC BANDS

In our calculations, we assume that lattice is composed of infinite number of unit cells. In our past work [12], we have numerically validated that the positions of the band gaps are not much affected by the finite size and small imperfection of the lattice. Dielectric function $\epsilon(\mathbf{r}, \varpi)$, in one unit cell, is given in Eq. (4).

In 2D PC there exist two independent modes [10]. When the **H/E** field is perpendicular to the plane of periodicity, the mode is called as transverse electric/magnetic, or by short hand notation TE/TM. We summarize the calculations here, but details can be found in [13].

The spatial dependence in the Master (eigenvalue) equation

$$\nabla \times \left(\frac{1}{\epsilon(\mathbf{r}, \omega)}\nabla \times \mathbf{H}(\mathbf{r})\right) = \left(\frac{\omega}{c}\right)^2 \mathbf{H}(\mathbf{r}) \quad (5)$$

is decomposed into the plane waves, in accordance with the Bloch–Floquet theorem [27]. This way a matrix equation is obtained. Using the condition of the determinant of the matrix to be zero, the relation of ω–k is solved.

There exists two possible ways to construct a relation between ω and k. In the first, we put real-ω values as input and obtain the complex-ω values. In the second, we put real-k values and extract complex-ω values. The first method is useful when the spatial attenuation of the subject of interest is the spatial attenuation of the probe pulse. Second one is useful in determining the attenuation time.

The two approaches give parallel results [18], but cannot be connected (or compared) directly. We choose the real-ω/complex-k method. This is because we are curious about if the penetration depth is less or greater than a few tens of lattice cites. In other words, we ask for if the band gap is strong enough to stop the probe beam or it partially transmits it.

4. RESULTS AND DISCUSSION

4.1. Band Structures

When the dielectric function is frequency independent, $\epsilon(\omega) = \epsilon$, master Eq. (5) is scalable with the lattice parameter a. This makes the structure of the photonic bands, when expressed in terms of the scaled frequency $\omega' = \omega a/2\pi c$, independent of the lattice dimensions. Such a scaling, however, is not possible for the frequency-dependent dielectric response. This is because, susceptibilities (1) and (2) are altered with the ratio of γ and $2\pi c/a$. This introduces a new variable, both for theoretical and experimental usage, since a is continuously tunable in rotating BEC.

We use the tune ability of the lattice parameter a to obtain stronger stoppage at the enhancement frequency Ω_0 ($\varpi_0 = 1.22$ in Fig. 2).

We compute the photonic bands for two different dielectric functions, plotted in Figs. 2a and 2b, and present the results in Figs. 4 and 5, respectively. Figure 3a and 3b are respective intermediate-steps for Figs. 4 and 5, to be mentioned in the following paragraph.

Our method of approach is as follows. First, we obtain the constant dielectric bands, in Fig. 3, at the enhancement frequency $\epsilon = \epsilon(\Omega_0)$. At that frequency dielectric constant is real and polarization is strong, see Fig. 2. Second, we arrange the lattice parameter such that enhancement frequency is placed at the center of

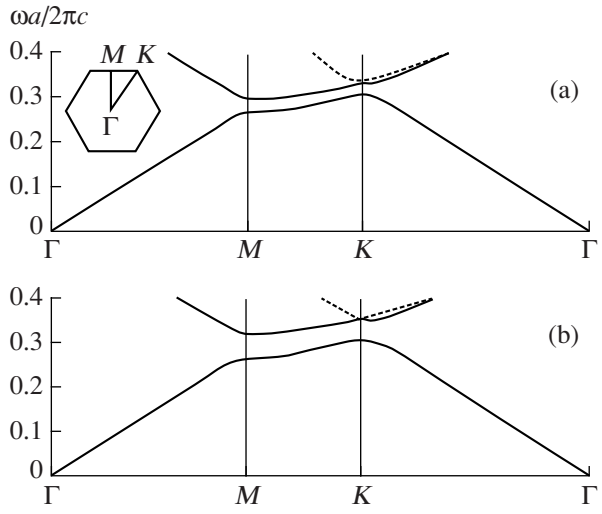

Fig. 3. TE modes of a triangular vortex lattice with frequency independent ϵ. (Symmetry points and the irreducible Brillouin zone of a triangular lattice are indicated in the inset.) Dielectric constants and lattice parameters are (a) $\epsilon = 5.2$ and $a = 10\xi$, (b) $\epsilon = 8$ and $a = 4.5\xi$. Filling fractions of vortices, $f = (2\pi/\sqrt{3}) \times (R^2/a^2)$ with effective radius $R \simeq 2\xi$, are 15 and 71%, respectively. Dielectric constant is the value of dielectric function (4) at the enhancement frequency, $\epsilon = \epsilon_{\rm loc}(\varpi_0)$. Density profile of the unit cell is treated using the Padé approximation [26]. (a) There exists a directional pseudo-band gap with midgap frequency at $\omega_g' = 0.285$. (b) There is a complete band gap with gap center at $\omega_g' = 0.31$.

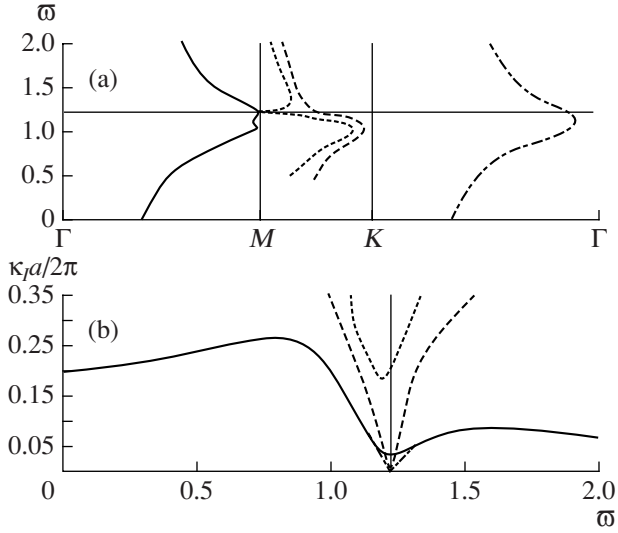

Fig. 4. (a) TE modes of triangular vortex lattice with frequency dependent dielectric function $\epsilon_{\rm loc}(\varpi)$ (Fig. 2), and (b) imaginary parts of the wave vector k_I corresponding to each mode. Particle density is $N = 5.5 \times 10^{20}$ m^{-3} and lattice constant is $a = 10\xi$. Enhancement frequency Ω_0 is tuned to the band gap at the M edge ($\omega_g = 0.285(2\pi c/a)$) of the constant dielectric case (Fig. 3a). MK bands are plotted in a limited region, because of high k_I values out of the given frequency region. There exists a directional gap in the ΓM propagation direction.

the gap. That is $\Omega_0 = \omega_g' (2\pi c/a)$, which gives the optimum lattice dimension as

$$a = \omega_g' \frac{2\pi c}{\omega_{ab} + \varpi_0 \gamma}. \quad (6)$$

Here, ω_g' is the scaled center of the gap frequency, to be read from constant dielectric bands of Fig. 3. Third, we obtain the photonic bands of frequency-dependent dielectric $\epsilon_{\rm loc}(\mathbf{r}, \varpi)$ of Eq. (4) in Figs. 4 and 5, with this arrangement.

In Fig. 3, we give the constant dielectric photonic bands of vortex lattice for two different parameter sets. The first set, $N = 5.5 \times 10^{20}$ m^{-3} and $a = 10\xi$, generates a directional pseudogap in the ΓM direction. Note that the value of dielectric constant, used in Fig. 3a, is the value of the dielectric function (Fig. 2a) at the enhancement frequency, $\epsilon = \epsilon_{\rm loc}(\varpi_0) = 5.2$. The a/ξ ratio determines the density profile in the hexagonal unit cell, according to function (3).

The dielectric band gap lies in the frequency range $\omega = (0.27–0.31)(2\pi c/a)$, with its center is at $\omega_g = 0.285(2\pi c/a)$. Then, in order to obtain the strongest stoppage at the enhancement frequency, we arrange the lattice constant to $a = 226$ nm according to (6). The resultant bands for the complex frequency-dependent dielectric response, depicted in Fig. 2a, is given in Fig. 4. The imaginary part of the wave vector, k_I, is also included.

The second parameter set, $N = 6.6 \times 10^{20}$ m^{-3} and $a = 4.5\xi$, is chosen such that there occurs a complete band gap, see Fig. 3, at the enhanced dielectric constant $\epsilon = \epsilon_{\rm loc}(\varpi_0) = 8$ (Fig. 2b). The complete gap lies in the frequency range $\omega = (0.30–0.32)(2\pi c/a)$, with the midgap frequency $\omega_g = 0.31(2\pi c/a)$. Note that, for the choice of $a = 4.5\xi$ filling factor of the vortex is higher. Then, for this parameter set, we arrange the lattice constant to $a = 246$ nm. Photonic bands for complex frequency-dependent dielectric function, which is plotted in Fig. 2b, is depicted in Fig. 5.

In Figs. 4a and 5a we plot the frequency with respect to the real part of the wave vector, k_R, for all bands. In Figs. 4b and 5b we give the imaginary parts of the wave vector, k_I, corresponding to each band. The enhancement frequency $\varpi_0 = 1.22$ is marked in all plots.

When the dielectric function is real, it is very easy to identify the band gaps. If there is propagation, k comes out to be real. If the frequency is in the band gap, k becomes complex, with k_R is on the band edge. In the case of complex $\epsilon(\omega)$, however, identification of the frequency range of the band gap is not straightforward. At a certain frequency, where ϵ is real, there exists a band gap, if k_I is nonzero. For other frequency values, where

ϵ is complex, the nonzero value of k_I may occur due to the absorption, as well as a reflector band gap. Even considering the gain regions about the enhancement frequency, ϖ_0 in Fig. 2, situation becomes more complicated. We discuss this in the following subsection, Section 4.2.

In Fig. 4b, imaginary parts of the wave vector k_I is plotted for different propagation directions. In the ΓM and ΓK directions only a single band exists within the enhancement window, while for the MK direction there are two bands. At the enhancement frequency $\varpi_0 = 1.22$, two of these bands have zero k_I, while the other two have a complex wave vector. In accordance with the discussion in the previous paragraph, we identify the existence of a pseudo-band gap in the ΓM propagation direction. Thus, incident light (exactly at ϖ_0) would propagate in the ΓK, MK directions while it would be stopped in the ΓM direction.

In the second case, Fig. 5, all of the four bands have nonzero k_I at $\varpi = \varpi_0$. This indicates the existence of a complete band gap at the enhancement frequency. Incident light is stopped for all propagation directions.

We see that the conclusions for the existence of photonic band gaps obtained by constant ϵ calculations are not modified, even when the strong frequency dependence of $\epsilon(\omega)$ is taken into account.

The reason of performing such a tuning, as in Eq. (6), is to keep the k_I maximum. The choice of ω_g', in Fig. 3, at the center of the gap is not obligatory. As long as ω_g' is chosen in the band gap of constant dielectric, there would be gap at $\varpi = \varpi_0$ in Figs. 4 and 5. But the stoppage, proportional to k_I, becomes smaller.

Here is worth to end this section by emphasizing the frequency dimensions of the enhancement window. Dielectric function (4) differs from the unity (vacuum) only in the frequency range $\omega = \Omega_0 \pm 5\gamma$ of width $\sim 10^9$ Hz. Since the typical lattice parameter in rotating BEC is about $a \sim 200$ nm, the natural lattice frequency $2\pi c/a$ is of order $\sim 10^{15}$ Hz. The later is six order of magnitude greater than the former. The index enhancement without absorption, on the other hand, is achievable in a narrower frequency range $\sim 0.1\gamma$. This illustrates the possible width of the band gaps.

4.2. Poynting Vector

We demonstrated the existence of both directional and complete band gap at exactly on the enhancement frequency Ω_0. The extent of the band gap about ω_0, however, cannot be argued considering only the k_I values. For a given value of k_I, one cannot distinguish between if the decaying behavior ($e^{-\mathbf{k}_I \cdot \mathbf{r}}$) is due to absorption or a band gap.

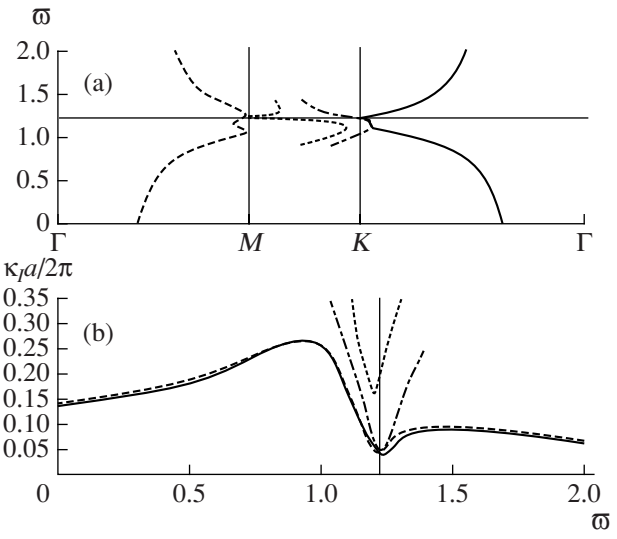

Fig. 5. (a) TE bands of triangular vortex lattice with frequency dependent dielectric function $\epsilon_{\text{loc}}(\varpi)$ (Fig. 2b), and (b) imaginary parts of the wave vector k_I corresponding to each mode. Particle density is $N = 6.6 \times 10^{20}$ m^{-3} and lattice constant is $a = 4.5\xi$. Enhancement frequency Ω_0 is tuned to the band gap at the M edge ($\omega_g = 0.31(2\pi c/a)$) of constant dielectric case (Fig. 3b). There exists a complete band gap.

To be able to define the width of the gap, we also examined the behavior of the complex Poynting vector

$$\mathbf{S}(\mathbf{r}) = \frac{1}{2}\mathbf{E}(\mathbf{r}) \times \mathbf{H}(\mathbf{r})^* \tag{7}$$

in the crystal. The real part of the Poynting vector, $\mathbf{S}_R(\mathbf{r})$, gives the energy flux of the field at position $\mathbf{r}$. On the other hand, imaginary part, $\mathbf{S}_I(\mathbf{r})$, is a measure of the reactive (stored) energy [28]. When $\epsilon(\omega)$ is real Poynting vector is real on the bands, and pure imaginary on the band gap regions. For a complex $\epsilon(\omega)$, however, the imaginary part of $\mathbf{S}$ may also be due to the absorption. Despite the similarity of the statements of $\mathbf{k}_I$ and $\mathbf{S}_I$, together they are sufficient in the determination of the gap width.

Fourier coefficients, corresponding to each frequency and band, are also calculated in the band computations. Using these coefficients, we calculated spatial average of the Poynting vector, $\langle \mathbf{S} \rangle$, in the unit cell. We define

$$\alpha = |\langle S_I \rangle| / |\langle S \rangle|, \tag{8}$$

as the rate of reactive (stored) energy. Since we aim to investigate the width of the directional gap in Fig. 4, $\langle S \rangle$ and $\langle S_I \rangle$ are computed along the ΓM direction.

The width of the gap is decided as follows. In Fig. 6, α displays a marked increase near the enhancement frequency. This increase, however, cannot be caused by the imaginary part of $\epsilon_{\text{loc}}(\varpi)$. Because, near the enhancement frequency this imaginary part decreases

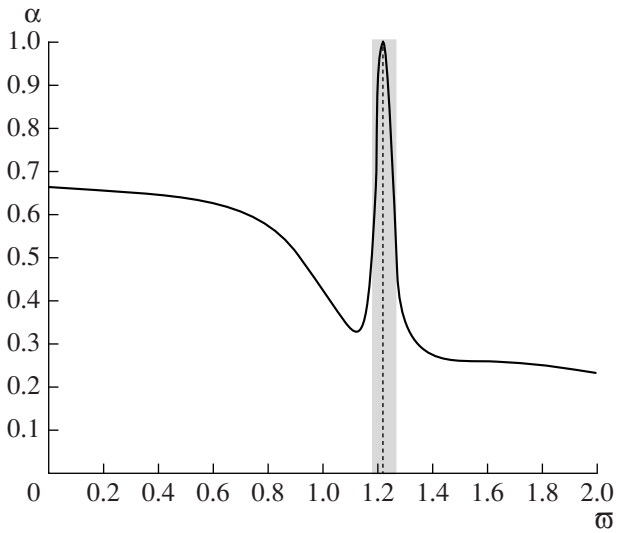

Fig. 6. Reactive energy ratio α for the Γ*M* band of Fig. 4. Vertical dashed line indicates the enhancement frequency $\varpi_0 = 1.22$. Shaded region is the effective photonic band gap. Width of the peak determines the width of the gap to be $\omega = \Omega \pm 0.043\gamma$ which corresponds to ±1.65 MHz.

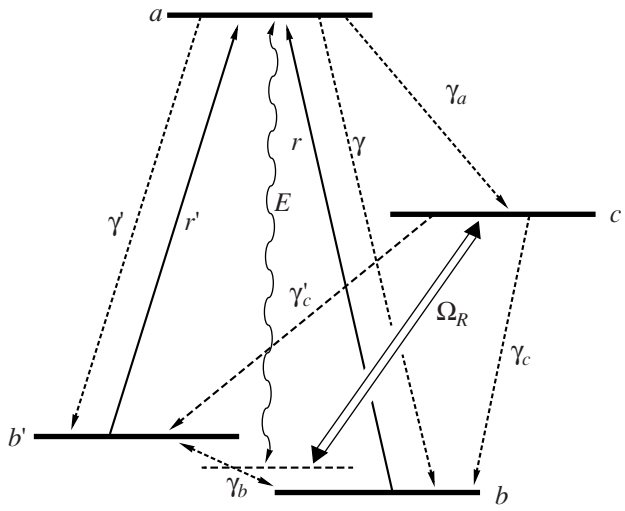

Fig. 7. Raman scheme for index enhancement. Probe field *E*, coupling field Ω_R, pumping rates *r*, *r*', and decay rates are indicated.

to zero. Thus, the peak in the reactive energy ratio must be cause by the periodicity of the crystal. The presence of the band gap increases the reactive energy ratio, despite the decreasing absorption.

We define the width of the band gap, in Fig. 6, as the full width at half maximum (FWHM) at the enhancement frequency. We note that at real dielectric, $\varpi = \varpi_0$, there is no propagation in the crystal ($\alpha = 1$) as expected. Within this definition, we determine an effective band gap in the frequency range $\varpi = \varpi_0 \pm 0.043$. This corresponds to a bandwidth of 3.30 MHz. The same method gives a band gap of width 5.98 MHz for the bands of Fig. 5.

Similar calculations for TM modes result in the similar band structure. Directional or complete band gaps are also achievable for TM modes. If the constant dielectric band gaps of TE and TM coincides, they also meat in the band structure of complex frequency-dependent dielectric case.

5. RAMAN SCHEME

The index enhancement in the upper-level microwave scheme is strong. However, vanishing absorption is achievable in only $0.04\gamma \simeq 3.3$ MHz frequency interval. In the Raman scheme [14], which is depicted in Fig. 7, the frequency interval of zero absorption is broader at least of one order of magnitude, see Fig. 8. The dielectric response, in contrast, is one order of magnitude weaker than the microwave scheme [14]. Then, microwave scheme provides a strong band gap (large k_I) at single frequency, but Raman scheme leads a weaker band gap (small k_I) at broader frequency interval.

Dielectric function for the Raman scheme is calculated numerically by solving density matrix equations in the steady state [14] and the results are plotted in the Fig. 8. We take the decay rates of the level *a* onto *b* and *b*' equal, since the levels are energetically very close. Because of the same reason, their decay in between is small $\gamma_b = \gamma_{b'} = 10^{-3}\gamma$. The spacing between the *b*–*b*' is $\omega_{bb'} = \gamma = \gamma'$. The decay rate of level *c* on *b* and *b*' is $\gamma_c = \gamma'_c = \gamma$. Since the *a*–*c* transition is dipole forbidden, $\gamma_a = 10^{-3}\gamma$. The Rabi frequency is $\Omega_R = 5.9\gamma$ and the pump rates are $r = r' = 0.017\gamma$. In Fig. 8, we indicated the frequency region of zero absorption with shadow. Between $\varpi = 1.8$–2.2 imaginary part χ'' vanishes. The new enhancement is about the frequency $\varpi_0 = 2$. The

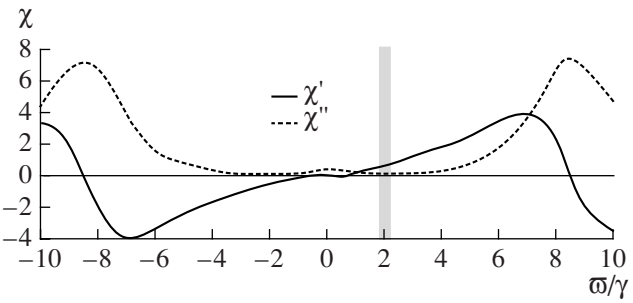

Fig. 8. Real (solid-line) and imaginary (doted-line) parts of dielectric function, obtained through Raman scheme for particle density $N = 2.3 \times 10^{23}$ m^{-3}. Shaded area, $\varpi = 1.8$–2.2, is the frequency window of zero absorption.

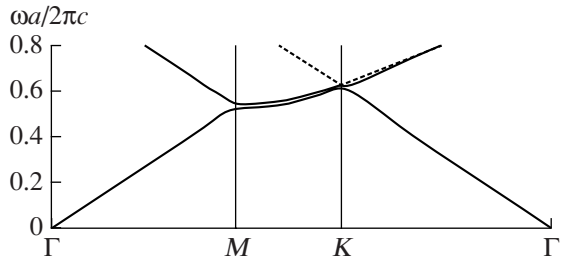

Fig. 9. Band diagram for TE modes of a triangular vortex lattice with frequency independent $\epsilon = 1.29$ and $a = 10\xi$. Midgap frequency is $0.537(2\pi c/a)$.

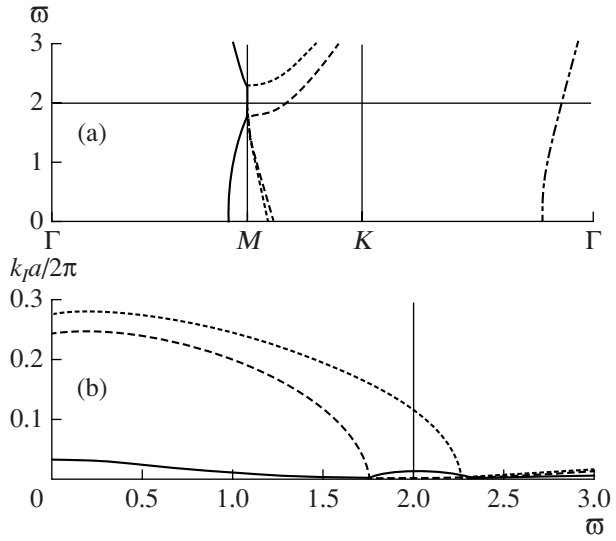

Fig. 10. TE bands of triangular vortex lattice with Raman index enhancement scheme, dielectric function plotted in Fig. 8. There exists a directional gap in the Γ*M* direction of width $0.4\gamma = 31$ MHz.

density used is 500 times of the one used in the upper-level microwave scheme, Fig. 2a.

In Fig. 9, frequency independent dielectric constant is used in the band calculation for the Raman scheme. Dielectric constant is chosen at the frequency in the middle of the zero-absorption window, shaded region in the Fig. 8.

In Fig. 10 we plotted the photonic bands of a triangular vortex lattice, where index enhancement is achieved via Raman scheme, taking into account frequency dependent complex dielectric function. In the calculation we followed the same methods, described in the Subsection 4.1. There is only a directional band gap in the Γ*M* direction. The frequency width of the gap is clear. There exists band gap in the whole frequency region $\varpi = 1.8$–2.2. This corresponds to a frequency width of $0.4\gamma = 31$ MHz. The stoppage of the incident pulse is accomplished after a propagation of about 80 cites.

6. CONCLUSIONS

We calculated the photonic bands for an index enhanced vortex lattice, considering a frequency dependent complex dielectric function. We review the main conclusions of our previous works [12, 13], that photonic band gaps can be created via index enhancement on vortex lattices of BECs. Specifically, we presented two examples showing that both directional and complete band gaps are possible within experimentally realizable parameter regimes. For the specific parameters and the upper level microwave scheme for index enhancement we considered, band gaps of order a few megahertz width are obtained. We also discussed how band gaps are designed for specific parameter values, and how band gap widths can be increased. In particular, using a Raman scheme allows for an order of magnitude increase in the band width.

ACKNOWLEDGMENTS

M.Ö.O. is supported by a TÜBA/GEBİP grant and TÜBİTAK-KARİYER Grant no. 104T165.

REFERENCES

1. J. R. AboShaeer, C. Raman, J. M. Vogels, and W. Ketterle, Science **292**, 476 (2001).
2. P. C. Haljan, I. Coddington, P. Engels, and E. A. Cornell, Phys. Rev. Lett. **87**, 210403 (2001).
3. T.-L. Ho, Phys. Rev. Lett. **87**, 060403 (2001).
4. G. Baym and C. J. Pethick, Phys. Rev. A **69**, 043619 (2004).
5. V. Schweikhard, I. Coddington, P. Engels, S. Tung, and E. A. Cornell, Phys. Rev. Lett. **93**, 210403 (2004).
6. P. Engels, I. Coddington, P. C. Haljan, and E. A. Cornell, Phys. Rev. Lett. **89**, 100403 (2002).
7. K. W. Madison, F. Chevy, W. Wohlleben, and J. Dalibard, Phys. Rev. Lett. **84**, 806 (2000).
8. K. W. Madison, F. Chevy, V. Bretin, and J. Dalibard, Phys. Rev. Lett. **86**, 4443 (2001).
9. N. L. Smith, W. H. Heathcote, J. M. Krueger, and C. J. Foot, Phys. Rev. Lett. **93**, 080406 (2004).
10. J. D. Joannopoulos, R. D. Meade, and J. N. Winn, *Photonic Crystals: Molding the Flow of Light* (Princeton Univ., Princeton, 1995).
11. S. L. Cornish, N. R. Claussen, J. L. Roberts, E. A. Cornell, and C. E. Wieman, Phys. Rev. Lett. **85**, 1795 (2000).
12. Ö. E. Müstecaplıoğlu and M. Ö. Oktel, Phys. Rev. Lett. **94**, 220404 (2005).
13. M. E. Taşgın, Ö. E. Müstecaplıoğlu, and M. Ö. Oktel, Phys. Rev. A **75**, 063627 (2007).
14. M. Fleischhauer, C. H. Keitel, M. O. Scully, C. Su, B. T. Ulrich, and S. Y. Zhu, Phys. Rev. A **46**, 1468 (1992).
15. M. O. Scully and M. S. Zubairy, *Quantum Optics* (Cambridge Univ., Cambridge, 1997).
16. A. A. Krokhin and P. Halevi, Phys. Rev. B **53**, 1205 (1996).

17. M. M. Sigalas, C. M. Soukoulis, C. T. Chan, and K. M. Ho, Phys. Rev. B **49**, 11080 (1994).

18. V. Kuzmiak and A. A. Maradudin, Phys. Rev. **55**, 7427 (1997).

19. L.-M. Li, Z.-Q. Zhang, and X. Zhang, Phys. Rev. B **58**, 15589 (1998).

20. A. Moroz, A. Tip, and J.-M. Combes, Synthetic Mat. (in press, 2009).

21. A. Tip, A. Moroz, and J.-M. Combes, J. Phys. A: Math. Gen. **33**, 6223 (2000).

22. H. van der Lem, A. Tip, and A. Moroz, J. Opt. Soc. Am. B **20**, 1334 (2003).

23. X. Jiang and C. M. Soukoulis, Phys. Rev. B **59**, 6159 (1999).

24. G. Veronis, R. W. Dutton, and S. Fan, J. App. Phys. **97**, 093104 (2005).

25. J. Ruostekoski and J. Javanainen, Phys. Rev. Lett. **82**, 4741 (1999); M. Fleischhauer, Phys. Rev. A **60**, 2534 (1999); H. Wallis, Phys. Rev. A **56**, 2060 (1997); O. Morice, Y. Castin, and J. Dalibard, Phys. Rev. A **51**, 3896 (1995); J. Ruostekoski and J. Javanainen, Phys. Rev. A **56**, 2056 (1997); K. V. Krutitsky, K.-P. Marzlin, and J. Audretsch, Phys. Rev. A **65**, 063609 (2002).

26. N. G. Berloff, J. Phys. A **37**, 1617 (2004).

27. A. Tip, A. Moroz, and J. M. Combes, J. Phys. A **33**, 6223 (2000); C. Kittel, *Introduction to Solid State Physics* (Wiley, New York, 1996).

28. J. D. Jackson, *Classical Electrodynamics* (Wiley, New York, 1999).